

Isolated Photon Cross Section in the Central and Forward Rapidity Regions in $p\bar{p}$ Collisions at $\sqrt{s} = 1.8$ TeV

- S. Abachi,¹⁴ B. Abbott,²⁸ M. Abolins,²⁵ B. S. Acharya,⁴⁴ I. Adam,¹² D. L. Adams,³⁷ M. Adams,¹⁷ S. Ahn,¹⁴
 H. Aihara,²² J. Alitti,⁴⁰ G. Álvarez,¹⁸ G. A. Alves,¹⁰ E. Amidi,²⁹ N. Amos,²⁴ E. W. Anderson,¹⁹ S. H. Aronson,⁴
 R. Astur,⁴² R. E. Avery,³¹ M. M. Baarmand,⁴² A. Baden,²³ V. Balamurali,³² J. Balderston,¹⁶ B. Baldin,¹⁴ S. Banerjee,⁴⁴
 J. Bantly,⁵ J. F. Bartlett,¹⁴ K. Bazizi,³⁹ J. Bendich,²² S. B. Beri,³⁴ I. Bertram,³⁷ V. A. Bezzubov,³⁵ P. C. Bhat,¹⁴
 V. Bhatnagar,³⁴ M. Bhattacharjee,¹³ A. Bischoff,⁹ N. Biswas,³² G. Blazey,¹⁴ S. Blessing,¹⁵ P. Bloom,⁷ A. Boehnlein,¹⁴
 N. I. Bojko,³⁵ F. Borcherding,¹⁴ J. Borders,³⁹ C. Boswell,⁹ A. Brandt,¹⁴ R. Brock,²⁵ A. Bross,¹⁴ D. Buchholz,³¹
 V. S. Burtovoi,³⁵ J. M. Butler,³ W. Carvalho,¹⁰ D. Casey,³⁹ H. Castilla-Valdez,¹¹ D. Chakraborty,⁴² S.-M. Chang,²⁹
 S. V. Chekulaev,³⁵ L.-P. Chen,²² W. Chen,⁴² S. Choi,⁴¹ S. Chopra,²⁴ B. C. Choudhary,⁹ J. H. Christenson,¹⁴
 M. Chung,¹⁷ D. Claes,⁴² A. R. Clark,²² W. G. Cobau,²³ J. Cochran,⁹ W. E. Cooper,¹⁴ C. Cretesinger,³⁹ D. Cullen-Vidal,⁵
 M. A. C. Cummings,¹⁶ D. Cutts,⁵ O. I. Dahl,²² K. De,⁴⁵ M. Demarteau,¹⁴ N. Denisenko,¹⁴ D. Denisov,¹⁴ S. P. Denisov,³⁵
 H. T. Diehl,¹⁴ M. Diesburg,¹⁴ G. Di Loreto,²⁵ R. Dixon,¹⁴ P. Draper,⁴⁵ J. Drinkard,⁸ Y. Ducros,⁴⁰ S. R. Dugad,⁴⁴
 D. Edmunds,²⁵ J. Ellison,⁹ V. D. Elvira,⁴² R. Engelmann,⁴² S. Eno,²³ G. Eppley,³⁷ P. Ermolov,²⁶ O. V. Eroshin,³⁵
 V. N. Evdokimov,³⁵ S. Fahey,²⁵ T. Fahland,⁵ M. Fatyga,⁴ M. K. Fatyga,³⁹ J. Featherly,⁴ S. Feher,⁴² D. Fein,²
 T. Ferbel,³⁹ G. Finocchiaro,⁴² H. E. Fisk,¹⁴ Y. Fisyak,⁷ E. Flattum,²⁵ G. E. Forden,² M. Fortner,³⁰ K. C. Frame,²⁵
 P. Franzini,¹² S. Fuess,¹⁴ E. Gallas,⁴⁵ A. N. Galyaev,³⁹ T. L. Geld,²⁵ R. J. Genik II,²⁵ K. Genser,¹⁴ C. E. Gerber,¹⁴
 B. Gibbard,⁴ V. Glebov,³⁹ S. Glenn,⁷ J. F. Glicenstein,⁴⁰ B. Gobbi,³¹ M. Goforth,¹⁵ A. Goldschmidt,²² B. Gómez,¹
 G. Gómez,²³ P. I. Goncharov,³⁵ J. L. González Solís,¹¹ H. Gordon,⁴ L. T. Goss,⁴⁶ N. Graf,⁴ P. D. Grannis,⁴²
 D. R. Green,¹⁴ J. Green,³⁰ H. Greenlee,¹⁴ G. Griffin,⁸ N. Grossman,¹⁴ P. Grudberg,²² S. Grünendahl,³⁹ W. X. Gu,^{14,*}
 G. Guglielmo,³³ J. A. Guida,² J. M. Guida,⁵ W. Guryn,⁴ S. N. Gurzhiev,³⁵ P. Gutierrez,³³ Y. E. Gutnikov,³⁵
 N. J. Hadley,²³ H. Haggerty,¹⁴ S. Hagopian,¹⁵ V. Hagopian,¹⁵ K. S. Hahn,³⁹ R. E. Hall,⁸ S. Hansen,¹⁴ R. Hatcher,²⁵
 J. M. Hauptman,¹⁹ D. Hedin,³⁰ A. P. Heinson,⁹ U. Heintz,¹⁴ R. Hernández-Montoya,¹¹ T. Heuring,¹⁵ R. Hirosky,¹⁵
 J. D. Hobbs,¹⁴ B. Hoeneisen,^{1,†} J. S. Hoftun,⁵ F. Hsieh,²⁴ Tao Hu,^{14,*} Ting Hu,⁴² Tong Hu,¹⁸ T. Huehn,⁹ S. Igarashi,¹⁴
 A. S. Ito,¹⁴ E. James,² J. Jaques,³² S. A. Jerger,²⁵ J. Z.-Y. Jiang,⁴² T. Joffe-Minor,³¹ H. Johari,²⁹ K. Johns,²
 M. Johnson,¹⁴ H. Johnstad,⁴³ A. Jonckheere,¹⁴ M. Jones,¹⁶ H. Jöstlein,¹⁴ S. Y. Jun,³¹ C. K. Jung,⁴² S. Kahn,⁴
 G. Kalbfleisch,³³ J. S. Kang,²⁰ R. Kehoe,³² M. L. Kelly,³² L. Kerth,²² C. L. Kim,²⁰ S. K. Kim,⁴¹ A. Klatchko,¹⁵
 B. Klima,¹⁴ B. I. Klochkov,³⁵ C. Klopfenstein,⁷ V. I. Klyukhin,³⁵ V. I. Kochetkov,³⁵ J. M. Kohli,³⁴ D. Koltick,³⁶
 A. V. Kostritskiy,³⁵ J. Kotcher,⁴ J. Kourlas,²⁸ A. V. Kozelov,³⁵ E. A. Kozlovski,³⁵ M. R. Krishnaswamy,⁴⁴
 S. Krzywdzinski,¹⁴ S. Kunori,²³ S. Lami,⁴² G. Landsberg,¹⁴ J.-F. Lebrat,⁴⁰ A. Leflat,²⁶ H. Li,⁴² J. Li,⁴⁵ Y. K. Li,³¹
 Q. Z. Li-Demarteau,¹⁴ J. G. R. Lima,³⁸ D. Lincoln,²⁴ S. L. Linn,¹⁵ J. Linnemann,²⁵ R. Lipton,¹⁴ Y. C. Liu,³¹
 F. Lobkowicz,³⁹ S. C. Loken,²² S. Lökö,⁴² L. Lueking,¹⁴ A. L. Lyon,²³ A. K. A. Maciel,¹⁰ R. J. Madaras,²²
 R. Madden,¹⁵ S. Mani,⁷ H. S. Mao,^{14,*} S. Margulies,¹⁷ R. Markeloff,³⁰ L. Markovsky,² T. Marshall,¹⁸ M. I. Martin,¹⁴
 B. May,³¹ A. A. Mayorov,³⁵ R. McCarthy,⁴² T. McKibben,¹⁷ J. McKinley,²⁵ T. McMahon,³³ H. L. Melanson,¹⁴
 J. R. T. de Mello Neto,³⁸ K. W. Merritt,¹⁴ H. Miettinen,³⁷ A. Mincer,²⁸ J. M. de Miranda,¹⁰ C. S. Mishra,¹⁴
 N. Mokhov,¹⁴ N. K. Mondal,⁴⁴ H. E. Montgomery,¹⁴ P. Mooney,¹ H. da Motta,¹⁰ M. Mudan,²⁸ C. Murphy,¹⁷ F. Nang,⁵
 M. Narain,¹⁴ V. S. Narasimham,⁴⁴ A. Narayanan,² H. A. Neal,²⁴ J. P. Negret,¹ E. Neis,²⁴ P. Nemethy,²⁸ D. Nešić,⁵
 M. Nichola,¹⁰ D. Norman,⁴⁶ L. Oesch,²⁴ V. Oguri,³⁸ E. Oltman,²² N. Oshima,¹⁴ D. Owen,²⁵ P. Padley,³⁷ M. Pang,¹⁹
 A. Para,¹⁴ C. H. Park,¹⁴ Y. M. Park,²¹ R. Partridge,⁵ N. Parua,⁴⁴ M. Paterno,³⁹ J. Perkins,⁴⁵ A. Peryshkin,¹⁴ M. Peters,¹⁶
 H. Piekarz,¹⁵ Y. Pischalnikov,³⁶ V. M. Podstavkov,³⁵ B. G. Pope,²⁵ H. B. Prosper,¹⁵ S. Protopopescu,⁴ D. Pušeljić,²²
 J. Qian,²⁴ P. Z. Quintas,¹⁴ R. Raja,¹⁴ S. Rajagopalan,⁴² O. Ramirez,¹⁷ M. V. S. Rao,⁴⁴ P. A. Rapidis,¹⁴ L. Rasmussen,⁴²
 A. L. Read,¹⁴ S. Reucroft,²⁹ M. Rijssenbeek,⁴² T. Rockwell,²⁵ N. A. Roe,²² P. Rubinov,³¹ R. Ruchti,³² J. Rutherford,²
 A. Santoro,¹⁰ L. Sawyer,⁴⁵ R. D. Schamberger,⁴² H. Schellman,³¹ J. Sculli,²⁸ E. Shabalina,²⁶ C. Shaffer,¹⁵
 H. C. Shankar,⁴⁴ R. K. Shrivpuri,¹³ M. Shupe,² J. B. Singh,³⁴ V. Sirotenko,³⁰ W. Smart,¹⁴ A. Smith,² R. P. Smith,¹⁴
 R. Snihur,³¹ G. R. Snow,²⁷ J. Snow,³³ S. Snyder,⁴ J. Solomon,¹⁷ P. M. Sood,³⁴ M. Sosebee,⁴⁵ M. Souza,¹⁰
 A. L. Spadafora,²² R. W. Stephens,⁴⁵ M. L. Stevenson,²² D. Stewart,²⁴ D. A. Stoianova,³⁵ D. Stoker,⁸ K. Streets,²⁸
 M. Strovink,²² A. Sznajder,¹⁰ P. Tamburello,²³ J. Tarazi,⁸ M. Tartaglia,¹⁴ T. L. Taylor,³¹ J. Thompson,²³ T. G. Tripp,²²
 P. M. Tuts,¹² N. Varelas,²⁵ E. W. Varnes,²² P. R. G. Virador,²² D. Vititoe,² A. A. Volkov,³⁵ A. P. Vorobiev,³⁵
 H. D. Wahl,¹⁵ G. Wang,¹⁵ J. Warchol,³² G. Watts,⁵ M. Wayne,³² H. Weerts,²⁵ F. Wen,¹⁵ A. White,⁴⁵ J. T. White,⁴⁶

J. A. Wightman,¹⁹ J. Wilcox,²⁹ S. Willis,³⁰ S. J. Wimpenny,⁹ J. V. D. Wirjawan,⁴⁶ J. Womersley,¹⁴ E. Won,³⁹
 D. R. Wood,²⁹ H. Xu,⁵ R. Yamada,¹⁴ P. Yamin,⁴ C. Yanagisawa,⁴² J. Yang,²⁸ T. Yasuda,²⁹ P. Yepes,³⁷
 C. Yoshikawa,¹⁶ S. Youssef,¹⁵ J. Yu,¹⁴ Y. Yu,⁴¹ Q. Zhu,²⁸ Z. H. Zhu,³⁹ D. Zieminska,¹⁸ A. Ziemiński,¹⁸
 E. G. Zverev,²⁶ and A. Zylberstejn⁴⁰
 (D0 Collaboration)

¹Universidad de los Andes, Bogotá, Colombia

²University of Arizona, Tucson, Arizona 85721

³Boston University, Boston, Massachusetts 02215

⁴Brookhaven National Laboratory, Upton, New York 11973

⁵Brown University, Providence, Rhode Island 02912

⁶Universidad de Buenos Aires, Buenos Aires, Argentina

⁷University of California, Davis, California 95616

⁸University of California, Irvine, California 92717

⁹University of California, Riverside, California 92521

¹⁰LAFEX, Centro Brasileiro de Pesquisas Físicas, Rio de Janeiro, Brazil

¹¹CINVESTAV, Mexico City, Mexico

¹²Columbia University, New York, New York 10027

¹³Delhi University, Delhi, India 110007

¹⁴Fermi National Accelerator Laboratory, Batavia, Illinois 60510

¹⁵Florida State University, Tallahassee, Florida 32306

¹⁶University of Hawaii, Honolulu, Hawaii 96822

¹⁷University of Illinois at Chicago, Chicago, Illinois 60607

¹⁸Indiana University, Bloomington, Indiana 47405

¹⁹Iowa State University, Ames, Iowa 50011

²⁰Korea University, Seoul, Korea

²¹Kyungsung University, Pusan, Korea

²²Lawrence Berkeley National Laboratory and University of California, Berkeley, California 94720

²³University of Maryland, College Park, Maryland 20742

²⁴University of Michigan, Ann Arbor, Michigan 48109

²⁵Michigan State University, East Lansing, Michigan 48824

²⁶Moscow State University, Moscow, Russia

²⁷University of Nebraska, Lincoln, Nebraska 68588

²⁸New York University, New York, New York 10003

²⁹Northeastern University, Boston, Massachusetts 02115

³⁰Northern Illinois University, DeKalb, Illinois 60115

³¹Northwestern University, Evanston, Illinois 60208

³²University of Notre Dame, Notre Dame, Indiana 46556

³³University of Oklahoma, Norman, Oklahoma 73019

³⁴University of Panjab, Chandigarh 16-00-14, India

³⁵Institute for High Energy Physics, 142-284 Protvino, Russia

³⁶Purdue University, West Lafayette, Indiana 47907

³⁷Rice University, Houston, Texas 77251

³⁸Universidade Estadual do Rio de Janeiro, Brazil

³⁹University of Rochester, Rochester, New York 14627

⁴⁰CEA, DAPNIA/Service de Physique des Particules, CE-Saclay, France

⁴¹Seoul National University, Seoul, Korea

⁴²State University of New York, Stony Brook, New York 11794

⁴³SSC Laboratory, Dallas, Texas 75237

⁴⁴Tata Institute of Fundamental Research, Colaba, Bombay 400005, India

⁴⁵University of Texas, Arlington, Texas 76019

⁴⁶Texas A&M University, College Station, Texas 77843

(Received 21 March 1996)

A measurement of the cross section for production of single, isolated photons is reported for transverse energies in the range of 10–125 GeV for two regions of pseudorapidity, $|\eta| < 0.9$ and $1.6 < |\eta| < 2.5$. The data represent 12.9 pb^{-1} of integrated luminosity accumulated in $\bar{p}p$ collisions at $\sqrt{s} = 1.8 \text{ TeV}$ and recorded with the D0 detector at the Fermilab Tevatron Collider. The background, predominantly from jets which fragment to neutral mesons, is estimated using the longitudinal shower shape in the calorimeter. In both pseudorapidity regions the cross section is found to agree with the next-to-leading order QCD prediction for $30 \lesssim E_T^\gamma \lesssim 80 \text{ GeV}$. [S0031-9007(96)01874-1]

PACS numbers: 13.85.Qk, 12.38.Qk

Direct photon production probes the parton-parton interaction without the ambiguities associated with jet identification, fragmentation, and energy measurement. In $\bar{p}p$ collisions at $\sqrt{s} = 1.8$ TeV, the dominant mode of production for photons with low transverse energy E_T^γ is through gluon Compton scattering. The cross section is thus sensitive to the gluon distribution in the proton (and antiproton) at low momentum fractions x : as low as $x \sim 10^{-3}$ for $E_T^\gamma \geq 10$ GeV and pseudorapidity $\eta \leq 2.5$ ($\eta = -\ln \tan \frac{\theta}{2}$, where θ is the polar angle with respect to the proton beam).

Previous collider experiments, including UA2 [1] and CDF [2], have reported an excess of photons at low E_T^γ ($\lesssim 30$ GeV) compared with the next-to-leading order (NLO) QCD prediction. This may be explained by additional gluon radiation beyond that included in the NLO calculation [3], or by modified parton distributions and fragmentation contributions [4].

This Letter presents the first measurement of the cross section for production of isolated photons in $\bar{p}p$ collisions at $\sqrt{s} = 1.8$ TeV with pseudorapidity $1.6 < |\eta| < 2.5$, and a new measurement of the isolated photon cross section in the central region ($|\eta| < 0.9$).

Photons are identified in the D0 detector [5] using a uranium/liquid argon sampling calorimeter housed in a central and two forward cryostats. The calorimeters cover the region of $|\eta| \leq 4$ and have electromagnetic (EM) energy resolution $\sigma_E/E = 15\%/\sqrt{E(\text{GeV})} \oplus 0.3\%$. The EM section is segmented longitudinally into four layers (EM1–EM4) of 2, 2, 7, and $10 X_0$, and transversely into towers in pseudorapidity and azimuthal angle $\Delta\eta \times \Delta\phi = 0.1 \times 0.1$ (0.05×0.05 at shower maximum in EM3). The central and forward drift chambers in front of the calorimeter allow photons to be distinguished from electrons and photon conversions by ionization measurement.

The data presented here represent $12.9 \pm 0.7 \text{ pb}^{-1}$ of integrated luminosity recorded during 1992–1993. The detector used a three-level triggering system. The first level used scintillation counters near the beam pipe to detect an inelastic interaction; the second level summed the EM energy in calorimeter towers of size $\Delta\eta \times \Delta\phi = 0.2 \times 0.2$. The third level was a software trigger in which clusters of calorimeter cells were formed and loose cuts made on shower shape.

Candidate clusters were accepted within the regions $|\eta| < 0.9$ and $1.6 < |\eta| < 2.5$ in order to avoid calorimeter boundaries; in the central region they were also required to be more than 1.6 cm from azimuthal module boundaries. The event vertex was required to be within 50 cm of its nominal positions. The resulting acceptance is $A = 0.73 \pm 0.01$ (0.86 ± 0.01) in the central (forward) regions. To identify photon candidates, no drift chamber tracks were allowed within $\Delta\theta \times \Delta\phi \approx 0.2 \times 0.2$ radians between the calorimeter cluster and the primary vertex. The efficiency of this requirement was estimated to be 0.85 ± 0.01 (0.61 ± 0.03) in the central (forward) re-

gions. (The inefficiency is due to photon conversions and overlaps with charged tracks from the underlying event.) The cluster was required to have a shape consistent with that of a single EM shower, to have more than 96% of its energy in the EM section of the calorimeter, and to be isolated using a cut on the transverse energy in the annular region between $\mathcal{R} = \sqrt{\Delta\eta^2 + \Delta\phi^2} = 0.2$ and $\mathcal{R} = 0.4$ around the cluster: $E_T^{\mathcal{R} \leq 0.4} - E_T^{\mathcal{R} \leq 0.2} < 2$ GeV. Finally, the missing transverse energy of the event was required to be less than 20 GeV to reject electrons from $W \rightarrow e\nu$ decays and events with large amounts of calorimeter noise. The efficiency of these last three cuts was estimated as a function of E_T^γ using a detailed Monte Carlo simulation of the detector and verified using $Z \rightarrow ee$ events. Its value is 0.92 ± 0.03 (0.77 ± 0.06) at $E_T^\gamma = 40$ GeV for central (forward) photons.

The prompt photon signal suffers from copious backgrounds due to π^0 and η mesons produced in jets. While the bulk of this background is rejected by the selection criteria (especially the isolation requirement) substantial contamination remains, predominantly from fluctuations in jet fragmentation which lead to a single meson carrying most of the jet energy. For meson transverse energies above about 10 GeV, the showers from its two decay photons coalesce and mimic a single photon shower in the calorimeter.

The fraction of the remaining candidates which are genuine direct photons (the purity \mathcal{P}) was determined using the energy E_1 deposited in the first layer (EM1) of the calorimeter. Since neutral meson decays produce two photons the probability that at least one of them undergoes a conversion to an e^+e^- pair in the calorimeter cryostat and first absorber plate is roughly twice that for a single photon. Meson showers therefore start earlier than photon showers leading to larger E_1 . A typical distribution of $\log_{10}(E_1/E_{\text{total}})$ is shown in Fig. 1. The distribution is fit as the sum of a photon signal plus π^0 and η meson backgrounds. Fitting was done separately for the central and forward samples for each E_T^γ bin, using χ^2 minimization, and constraining the fractions of signal and background to lie in the range [0, 1]. The results presented use a production ratio of $\eta/\pi^0 = 1.0$ [6], but all values between 0.50 and 1.25 give essentially indistinguishable results for \mathcal{P} . The Monte Carlo calculation combines a detailed simulation of the calorimeter with overlaid minimum bias events from data to model noise, pileup, and the underlying event. Its ability to correctly model the E_1/E_{total} distribution has been verified using electrons from $W \rightarrow e\nu$ events taken with the same trigger requirements.

The combined statistical and systematic error on the purity \mathcal{P} at each E_T^γ point was estimated by inflating by $\sqrt{\chi^2}$ the error on \mathcal{P} given by the fit. The factor of $\sqrt{\chi^2}$ accounts for systematic differences between the Monte Carlo distributions and the data; it was typically 1.3 (1.6) in the central (forward) region. The photon purities were then corrected by the E_T^γ -dependent efficiencies and fit to

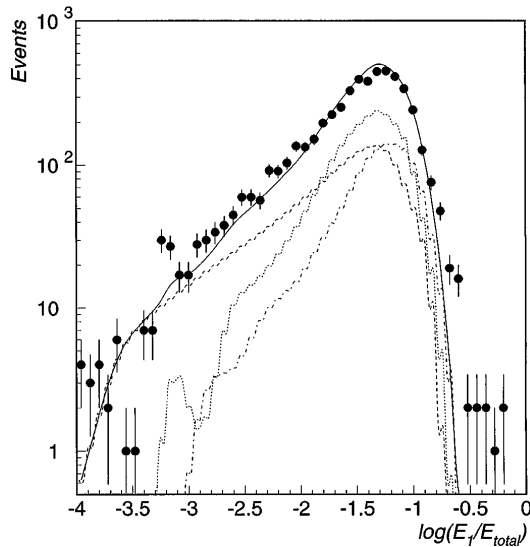


FIG. 1. Distribution of $\log_{10}(E_1/E_{\text{total}})$ for $E_T^\gamma = 40 \pm 5$ GeV central photon candidates (solid points), and the fitted distribution (solid curve) made up of Monte Carlo photons (dashes), π^0 (dots), and η mesons (dot-dashed curve). The π^0 and η meson distributions at small $\log_{10}(E_1/E_{\text{total}})$ fluctuate due to limited Monte Carlo statistics.

the form:

$$\mathcal{P} = 1 - e^{-(a+bE_T^\gamma)}. \quad (1)$$

The data points, fits, and fit errors for \mathcal{P} are shown in Fig. 2.

The purity estimation was checked with a second independent method, using the material between the interaction point and the central or forward drift chamber (CDC or FDC) as a converter. Conversions are identified as tracks with twice minimum ionizing deposition in the CDC or FDC. The second method gives consistent

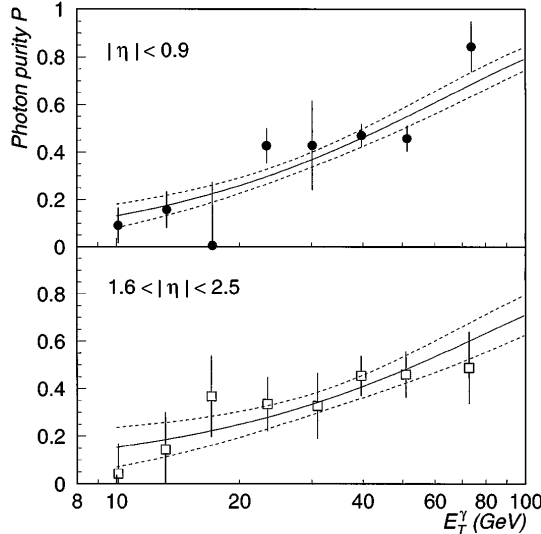


FIG. 2. Efficiency-corrected photon purity (\mathcal{P}) vs E_T^γ for central and forward photons. The solid lines show fits of the form $1 - e^{-(a+bE_T^\gamma)}$ and the dashed lines indicate the range of uncertainty thereon.

results, but has larger statistical errors, and therefore was not used in the fit.

The differential cross section $d^2\sigma/dE_T^\gamma d\eta$ is plotted as a function of E_T^γ in Fig. 3. The NLO QCD calculation was generated using a program due to Baer, Ohnemus, and Owens [7] which includes $\gamma + \text{jet}$, $\gamma + \text{dijet}$, and dijet + bremsstrahlung final states. In the latter case a collinear jet was created with the remaining jet energy, so that the isolation cut could be modeled. In all cases the parton energies were smeared using the measured D0 EM and jet resolutions. The isolation cut is imposed by rejecting events with a smeared jet $E_T > 2$ GeV within $\mathcal{R} \leq 0.4$ of the photon. (Use of smeared photon and jet energies changes the QCD prediction by less than 4%).

The CTEQ2M parton distributions [8] and renormalization scale $\mu = E_T^\gamma$ were used. If instead the CTEQ2MF or CTEQ2MS parton distributions were used, or scales of $\mu = 2E_T^\gamma$ or $E_T^\gamma/2$ were employed, then the predicted cross section changes by $\lesssim 6\%$.

Figure 4 shows $(\sigma_e - \sigma_t)/\sigma_t$ where σ_e and σ_t are, respectively, the experimental and theoretical values of the differential cross section $d^2\sigma/dE_T^\gamma d\eta$. The shaded band in Fig. 4 shows the magnitude of the combined systematic error, the quadratic sum of the uncertainties from the acceptance ($\sim 1\%$), the trigger and selection efficiencies (3%–5%), the photon purity (Fig. 3), the luminosity (5%), and the EM energy scale of the calorimeter (1% in the central, 4% in the forward region). In both central and forward regions, the measured cross sections are in good agreement with the NLO QCD prediction for moderate transverse energies, $30 \leq E_T^\gamma \leq 80$ GeV. The data points lie above the NLO QCD prediction at lower transverse energies, but given the magnitude of the systematic error no strong conclusion can be drawn. At the highest transverse energies

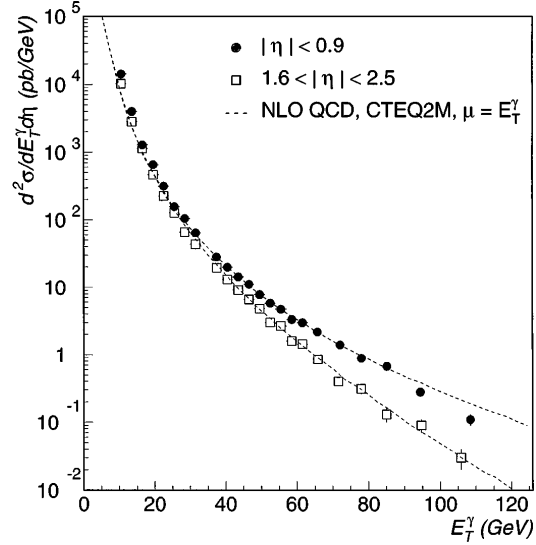


FIG. 3. The isolated photon cross section $\sigma_e = d^2\sigma/eE_T^\gamma d\eta$ as a function of photon transverse energy E_T^γ , for central (circles) and forward regions (squares). The errors are statistical only. The NLO QCD calculated cross sections σ_1 are also shown.

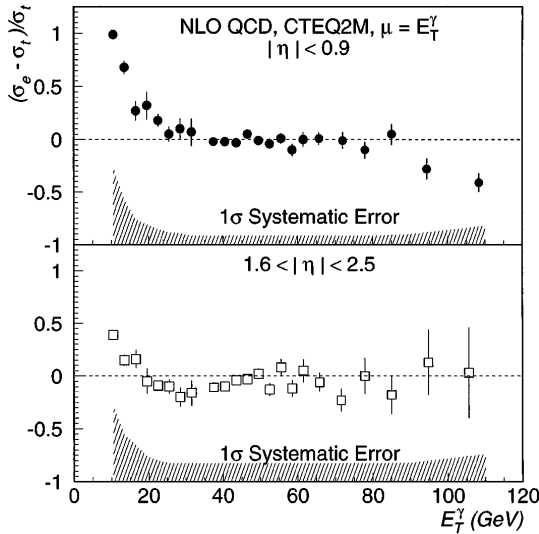


FIG. 4. Difference between the measured isolated photon cross section σ_t , normalized to the latter. The shaded bands show the magnitude of the systematic errors (1σ) for each of the two regions.

probed, the data for the central region lie below the QCD prediction. Above $E_T^\gamma = 74$ GeV the photon purity \mathcal{P} is the result of an extrapolation; the increased systematic error at large E_T^γ reflects the resulting uncertainty.

The ratio of forward to central cross sections is shown in Fig. 5. The systematic error on the ratio is obtained by adding those for the two regions in quadrature, with

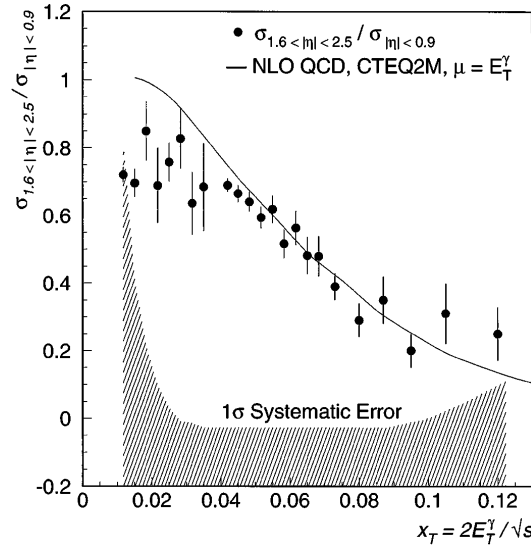


FIG. 5. Ratio of isolated photon cross sections $d^2\sigma/dx_T d\eta$ in the forward region to the central region. The NLO QCD prediction is also shown. The shaded band shows the magnitude of the systematic error.

the exception of the luminosity uncertainty which cancels. The data are in reasonable agreement with NLO QCD given the magnitude of the systematic error. This ratio, which exploits our unique measurement of the forward photon cross section, provides a new constraint on the gluon distribution, especially for $x \geq 0.03$ where the systematic errors are moderate. While not being sufficiently precise to distinguish, by itself, between modern parametrizations of the gluon distribution, this measurement complements previous ones and provides additional information for the extraction of parton distributions by global fitting of data. A more complete understanding of the origin of the low- E_T^γ behavior of the photon cross section is probably needed before information on the gluon distribution at lower x can be extracted.

We thank the Fermilab Accelerator, Computing, and Research Divisions, and the support staffs at the collaborating institutions for their contributions to the success of this work. We also acknowledge the support of the U.S. Department of Energy, the U.S. National Science Foundation, the Commissariat à L'Energie Atomique in France, the Ministry for Atomic Energy and the Ministry of Science and Technology Policy in Russia, CNPq in Brazil, the Departments of Atomic Energy and Science and Education in India, Colciencias in Colombia, CONACyT in Mexico, the Ministry of Education, Research Foundation and KOSEF in Korea, CONICET and UBACYT in Argentina, and the A. P. Sloan Foundation.

*Visitor from IHEP, Beijing, China.

†Visitor from Univ. San Francisco de Quito, Ecuador.

- [1] UA2 Collaboration, J. Alitti *et al.*, Phys. Lett. B **263**, 544 (1991).
- [2] CDF Collaboration, F. Abe *et al.*, Phys. Rev. D **48**, 2998 (1993); CDF Collaboration, F. Abe *et al.*, Phys. Rev. Lett. **73**, 2662 (1994).
- [3] J. Huston *et al.*, Phys. Rev. D **51**, 6139 (1995).
- [4] M. Glück, L. E. Gordon, E. Reya, and W. Vogelsang, Phys. Rev. Lett. **73**, 388 (1994); W. Vogelsang and A. Vogt, Nucl. Phys. **B453**, 334 (1995); E. Quack and D. K. Srivastava, Gesellschaft für Schwerionenforschung Report No. GSI-94-40, 1995 (to be published).
- [5] D0 Collaboration, S. Abachi *et al.*, Nucl. Instrum. Methods Phys. Res., Sect. A **338**, 185 (1994).
- [6] CDF Collaboration, F. Abe *et al.*, Phys. Rev. D **48**, 2998 (1993).
- [7] H. Baer, J. Ohnemus, and J. F. Owens, Phys. Rev. D **42**, 61 (1990).
- [8] CTEQ Collaboration, J. Botts *et al.*, Phys. Lett. B **304**, 159 (1993).